

Quantum conductance of helical nanowires

Masakuni Okamoto and Tsuyoshi Uda

Joint Research Center for Atom Technology (JRCAT)-Angstrom Technology Partnership (ATP), 1-1-1 Higashi, Tsukuba 305-0046, Japan

Kunio Takayanagi

Department of Material Science and Engineering, Tokyo Institute of Technology, 4259 Nagatsuta, Midori-ku, Yokohama 226-8502, Japan

(Received 23 February 2001; published 8 June 2001)

We have calculated the quantum conductance of N -fold helical metallic nanowires by using recursion-transfer-matrix method. When L_H (the pitch of the helix) is in a certain range, there appear characteristic humps and dips with steps of $1G_0$ or $2G_0$ ($G_0=2e^2/h$) in the conductance. The anomalous conductance originates from the fact that an energy gap opens due to noncircular cross section and shifts toward higher energies with decreasing L_H .

DOI: 10.1103/PhysRevB.64.033303

PACS number(s): 73.23.Ad, 73.21.-b, 73.40.Jn

Very recently, the gold nanowires were formed in gold thin films by electron-beam irradiation in an ultrahigh vacuum. Transmission electron microscopy images showed that they take helical configurations.¹ Prior to the experimental observation, using empirical molecular dynamics (MD), it was predicted that even for metals with isotropic atomic potentials, the helical structures could be stable when the diameters are smaller than the critical values.² More recent theoretical investigation revealed that the helical structures are stabilized as a result of optimization of surface and interior (bulk) energies.³

It is well recognized that the conductivity of carbon nanotubes changes drastically from metallic to semiconducting/insulating depending on the chirality of a tube.⁴⁻⁷ On the other hand, the conductance of the helical gold nanowires has not been measured yet. Therefore it is an interesting problem to clarify whether the similar conductance changes take place in metallic nanowires with helical configurations. In this paper, we study theoretically the conductance of the helical nanowires. We will demonstrate later that the quantum conductance shows enhancement and suppression depending on the pitch of the helix L_H but that it never becomes insulating.

We adopted the jellium model where electrons are confined in a uniform potential with boundary of the helical geometry as shown in Fig. 1. In spite of the simplicity of such a model, electronic properties of nanostructures have been successfully investigated, yielding a number of fruitful informations, for example, the quantized conductance varying with a unit of G_0 ($=2e^2/h$), oscillations in the tensile force as a function of the elongation of the wire, and the interplay between the size effect and the Landau splitting under magnetic field.⁸⁻¹¹ The shapes of cross sections were approximated by polygons, having N -fold symmetry with $N=5,6,7$, and ∞ (cylinder) as a reference. According to the MD simulations for Pb and Al nanowires, structures $N=5,6,7$ were often stabilized.² Experimentally, on the other hand, the thinnest helical gold nanowire was observed to have sevenfold symmetry.¹ The helical wire of length L_W was connected to jellium electrodes. We used electron density ($E_F=5.53$ eV) and the work function ($W_\phi=5.47$ eV) of gold s electrons. The potential depth (11.0 eV) was deter-

mined to give the above constants. The same area πR^2 of the cross section for each wire was assumed, where R is the averaged radius. We fixed R to be 0.53 nm as an example. Then the Sharvin's number $(\pi R/\lambda_F)^2=10.3$,¹² and we confirmed there existed ten quantized states below the Fermi level.

The Hamiltonian \hat{H}_{HN} of the wire is written as

$$\hat{H}_{HN} = \frac{1}{2}(\hat{p}_x^2 + \hat{p}_y^2 + \hat{p}_z^2) + V_{HN}(x, y, z), \quad (1)$$

where $(\hat{p}_x, \hat{p}_y, \hat{p}_z)$ are the momentum operators and $V_{HN}(x, y, z)$ is the effective potential of the helical wire, the cross section of which has N -fold symmetry. Atomic units are employed. When N is infinitely large (cylinder), eigenstates of the Hamiltonian $\hat{H}_{H\infty}$ can be solved analytically. They are specified by a set of quantum numbers (n, m, k_z) , where n, m are the principal and angular momentum quantum numbers and k_z is the momentum along the wire. For a finite integer N , however, m is no longer a good quantum number.

We first calculated the quantum conductance numerically by using recursion-transfer-matrix (RTM) method.¹³ In the RTM method, we consider a periodically repeated unit cell in the xy direction each containing the single wire of \hat{H}_{HN} . Due to the periodicity, wave function can be expressed by

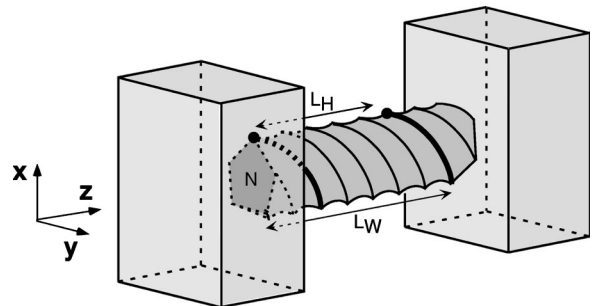


FIG. 1. Model of the helical nanowire. L_H is the pitch of the helix and L_W is the length of the wire. The helical nanowire is connected to jellium electrodes. The shape of the cross section is assumed to be an N -fold polygon.

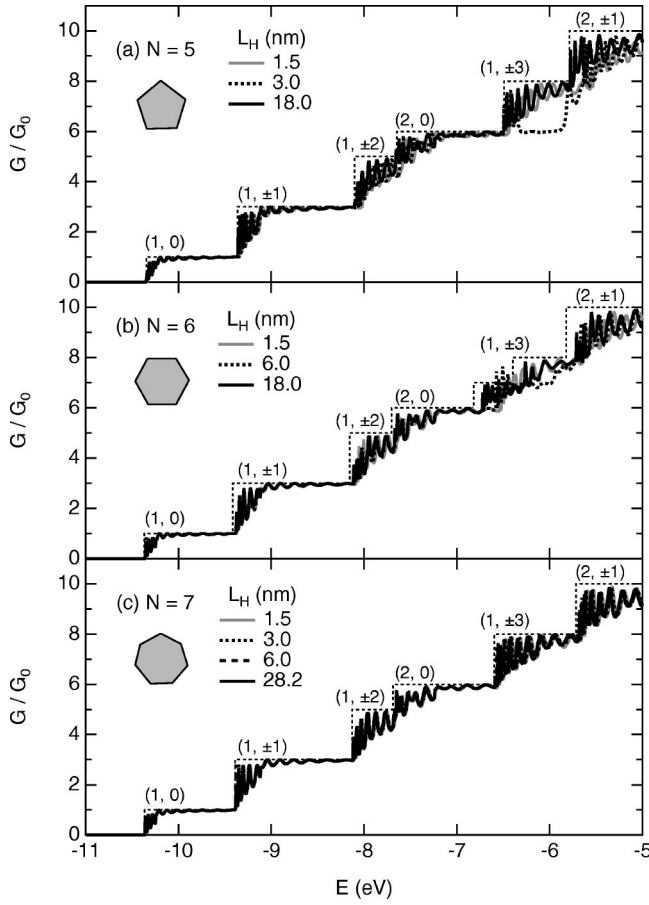


FIG. 2. Conductance curves numerically calculated by the RTM method as a function of electron energy E of helical nanowires for several helical pitches L_H of (a) $N=5$, (b) $N=6$, and (c) $N=7$. Stepwise broken lines show the conductance values for infinite L_H estimated by the Landauer formula. Quantum numbers (n, m) are shown for each conductance step.

$$\Psi_{\mathbf{k}_{\parallel}}(\mathbf{r}_{\parallel}, z) = e^{i\mathbf{k}_{\parallel}\mathbf{r}_{\parallel}} \sum_{\mathbf{G}_{\parallel}} u_{\mathbf{k}_{\parallel}}(\mathbf{G}_{\parallel}, z) e^{i\mathbf{G}_{\parallel}\mathbf{r}_{\parallel}}, \quad (2)$$

where \mathbf{k}_{\parallel} is the Bloch k vector and \mathbf{G}_{\parallel} is the reciprocal-lattice vector in the xy -Brillouin zone. The expansion is taken for \mathbf{G}_{\parallel} satisfying $\frac{1}{2}|\mathbf{k}_{\parallel} + \mathbf{G}_{\parallel}|^2 < E_{cut}$, where E_{cut} is the cutoff energy. The expansion coefficients $u_{\mathbf{k}_{\parallel}}(\mathbf{G}_{\parallel}, z)$ are solved by real-space discretization along z direction. A continued fraction formalism is used to eliminate numerically unstable components and the electric current and/or conductance can be calculated stably. The input parameters for numerical calculation are as follows¹⁴ if not stated otherwise; cutoff energy $E_{cut} = 40$ eV, mesh size $\Delta z = 0.05$ nm, length of the wire $L_W = 6.0$ nm (the same length as the gold nanowires formed experimentally¹), and the unit cell in the xy plane $L_x = L_y = 2.0$ nm. Only $\mathbf{k}_{\parallel} = 0$ point is used in the present calculation.

The numerical results are shown as a function of the electron energy E , in Fig. 2 for (a) $N=5$, (b) $N=6$, and (c) $N=7$ helical wires. The rapid oscillations of the calculated conductance curves are due to the interference between incident and reflected electrons.¹⁵ The periods of the oscillations

are of order $(2\pi/L_W)^2 \approx 0.08$ eV. We have confirmed that the periods became four times larger than the ones with half of L_W . Thus the oscillations are caused by the finite-size effect due to the existence of the electrodes. In real systems, since two contacts between wire and electrodes are smoother than the present model, the interference effect will be suppressed. The broken lines show maximum conductance values for infinite L_H obtained by the Landauer formula, where the interference effects are not considered. There are several characteristic features in the calculated conductance curves; (i) In case of $N=5$, a dip of depth $2G_0$ appears after the onset of the modes $(1, \pm 3)$ only for $L_H = 3.0$ nm. (ii) In case of $N=6$, conductance curve has a hump and a dip of depth $1G_0$ around the modes $(1, \pm 3)$ only for $L_H = 6.0$ nm. The two modes $(1, \pm 3)$ for infinite L_H are split, while they seem to be degenerate for small L_H . (iii) In case of $N=7$, all conductance curves coincide with each other, including $L_H = 28.2$ nm for the thinnest helical gold wire formed so far. In all cases, the wires do not become insulators. In order to check the accuracy of the numerical calculations, we have carried out for some cases more detailed calculations with using twice of E_{cut} and/or half of Δz . The results showed no significant changes. The anomalous behaviors stated above are not the artifacts arising from the numerical errors.

In order to interpret the characteristic features in the calculated conductance curves and to generalize the results, we analyzed eigenstates of the Hamiltonian \hat{H}_{HN} in the case of an infinitely long wire without electrodes. Introducing the new coordinates (x', y', z') defined as

$$\begin{aligned} x &= x' \cos \theta - y' \sin \theta, \\ y &= x' \sin \theta + y' \cos \theta, \\ z &= z', \end{aligned} \quad (3)$$

where $\theta \equiv G_H z$ with $G_H \equiv 2\pi/L_H$, the momentum operators $(\hat{p}_x, \hat{p}_y, \hat{p}_z)$ are transformed as

$$\begin{aligned} \hat{p}_x &= \hat{p}_{x'} \cos \theta - \hat{p}_{y'} \sin \theta, \\ \hat{p}_y &= \hat{p}_{x'} \sin \theta + \hat{p}_{y'} \cos \theta, \\ \hat{p}_z &= \hat{p}_{z'} - G_H \hat{L}_{z'}, \end{aligned} \quad (4)$$

where $\hat{L}_{z'}$ is the angular momentum operator. Then \hat{H}_{HN} is transformed into

$$\hat{H}'_{HN} = \frac{1}{2}(\hat{p}_{x'}^2 + \hat{p}_{y'}^2) + V_N(x', y') + \frac{1}{2}(\hat{p}_{z'} - G_H \hat{L}_{z'})^2. \quad (5)$$

In the new representation, V_N is independent on z' and the z' component of the momentum $k_{z'}$ becomes a good quantum number. However, because angular momentum operator $\hat{L}_{z'}$ does not commute with the potential $V_N(x', y')$, couplings occur between angular momentum states. We divided the Hamiltonian \hat{H}'_{HN} into two parts,

$$\hat{H}'_{HN} = \hat{H}'_{H\infty} + \Delta V_N, \quad (6)$$

where the first and the second terms are isotropic and anisotropic parts, respectively. The second term ΔV_N is

$$\Delta V_N(x', y') = V_N(x', y') - V_\infty(x', y') \quad (7)$$

by definition. Eigenfunctions and eigenvalues of $\hat{H}'_{H\infty}$ are expressed as

$$|nmk_{z'}\rangle = \psi_{nm}^\infty(r') e^{im\phi'} e^{ik_{z'}z'},$$

$$E_{nmk_{z'}} = E_{nm}^\infty + \frac{1}{2}(k_{z'} - mG_H)^2, \quad (8)$$

where ψ_{nm}^∞ and E_{nm}^∞ are the radial wave function and the two-dimensional energy level of the state (n, m) for a circular potential, respectively. Since the perturbation ΔV_N is a periodic function of ϕ' with a period $2\pi/N$, it can be expanded as

$$\Delta V_N(r', \phi') = \sum_j V_j^N(r') e^{iNj\phi'}, \quad (9)$$

where $V_j^N(r')$ is an expansion coefficient. The matrix element $\langle nmk_{z'} | \Delta V_N | n'm'k_{z'} \rangle$ vanishes except for the following cases:

$$m - m' = lN, \quad (10)$$

where l is an integer. No such selection rules exist between n and n' . In fact, the matrix elements are found to be the same order for different values of n and n' . It should be noted that as the helical pitch L_H decreases, low energy eigenstates of the total Hamiltonian \hat{H}'_{HN} approach those of a cylinder, because the energies where mixing occurs shift toward higher energies.

Since the energy separations between eigenmodes are relatively large in nanowires, it is sufficient to consider the couplings between only a few adjacent modes. At first we consider the case of two-mode coupling between the modes (n, m) and (n', m') , described by the following 2×2 matrix:

$$\begin{pmatrix} \tilde{E}_m^\infty + \frac{1}{2}(k_{z'} - mG_H)^2 & V_1 \\ V_1^* & \tilde{E}_{m'}^\infty + \frac{1}{2}(k_{z'} - m'G_H)^2 \end{pmatrix}, \quad (11)$$

where

$$\tilde{E}_m^\infty \equiv E_{nm}^\infty + \langle nmk_{z'} | \Delta V_N | nmk_{z'} \rangle,$$

$$\tilde{E}_{m'}^\infty \equiv E_{n'm'}^\infty + \langle n'm'k_{z'} | \Delta V_N | n'm'k_{z'} \rangle,$$

and

$$V_1 \equiv \langle nmk_{z'} | \Delta V_N | n'm'k_{z'} \rangle.$$

In Fig. 3, the analytical results are summarized. Several vari-

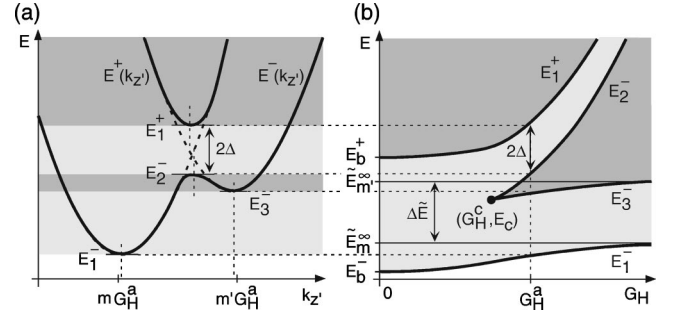


FIG. 3. Results of the two-mode coupling analysis between the modes (n, m) and (n', m') ; (a) band structure, and (b) the region with two eigenmodes (light gray) and four eigenmodes (dark gray) as a function of G_H . In the light gray region, the conductance increases by $1G_0$, while in the dark gray by $2G_0$. Energy gap 2Δ appears for $G_H \geq G_H^c$.

ables shown in the figure are defined as

$$\Delta \tilde{E} = \tilde{E}_{m'}^\infty - \tilde{E}_m^\infty,$$

$$E_b^\pm = \frac{1}{2}(\tilde{E}_m^\infty + \tilde{E}_{m'}^\infty) \pm \frac{1}{2}\sqrt{(\Delta \tilde{E})^2 + (2|V_1|)^2},$$

$$\frac{1}{2}(m - m')^2 (G_H^c)^2 = \{(\Delta \tilde{E})^2 + (2|V_1|)^2\}^{3/2}. \quad (12)$$

The eigenvalues $E^\pm(k_{z'})$ for intermediate G_H^a are illustrated in the left figure. A gap of 2Δ ($\approx 2|V_1|$) opens near the energy at the level crossing. As a result, there arises a new energy region with four eigenstates in the region with two eigenstates. They are shaded by dark gray and light gray, respectively. In the former region, the conductance increases by $2G_0$, while in the latter by $1G_0$. Variation of these regions with increasing G_H is shown in the right figure. When G_H is small, there exist two energy regions; the lower one has two eigenstates and the higher one has four eigenstates. At certain critical value of G_H^c , the region with four eigenstates emerges. With increasing G_H , the new energy region widens, keeping the width of the gap region nearly constant (2Δ). Eventually, the energy structure comes up to that of a cylinder.

All the complicated behaviors of the conductance in Fig. 2 can be understood by using Fig. 3(b). In case of $N=6$, energetically degenerate modes $(1, 3)$ and $(1, -3)$ couple each other. Since $\Delta \tilde{E} = 0$ eV in this case, the conductance due to these modes changes $0, 1G_0, 2G_0$ as a function of E for $L_H \geq L_H^c$, and changes $0, 2G_0, 1G_0, 2G_0$ for $L_H < L_H^c$. We obtain the critical point $(L_H^c, E_c) = (11.33 \text{ nm}, -6.71 \text{ eV})$ by the analytical expressions as in Eq. (12), together with the numerically obtained value $|V_1| = 0.21$ eV. We plot the analytical conductance neglecting the interface effect in Figs. 4(a), (b), (c) for $L_H = 5.0, 6.0, 7.0$ nm by gray lines. Also in the figure, conductance values calculated by the RTM method are plotted by the solid lines. The agreement is satisfactory. In case of $N=5$, the nearest modes which couple with the modes $(1, \pm 3)$ are $(1, \mp 2)$. In this

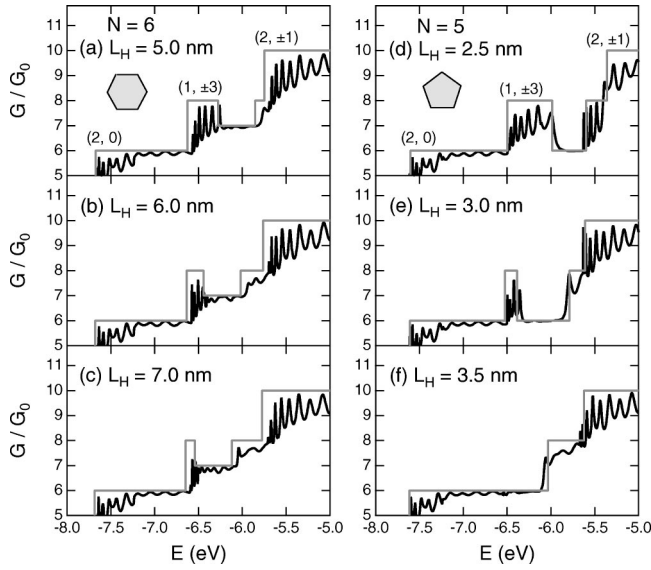


FIG. 4. Dependence of the conductance on the helical pitch L_H near the anomalous energy region. (a), (b), (c) are for $N=6$, and (d), (e), (f) are for $N=5$. Gray and solid lines show the results by the mode-coupling analysis and by the RTM method, respectively.

case, $\Delta\tilde{E}=1.48$ eV, $|V_1|=0.32$ eV, and $(L_H^c, E_c) = (3.58$ nm, -6.64 eV). The results of the two-mode coupling was qualitatively good, but they did not reproduce the results of RTM quantitatively. This is because there exist another modes $(2, \mp 2)$, which couple with the modes $(1, \pm 3)$, located at -3.66 eV (not shown in Fig. 2). Therefore we consider coupling of three modes by diagonalizing a 3×3 matrix and we obtain $2\Delta=0.65$ eV, and (L_H^c, E_c)

$= (3.49$ nm, -6.56 eV). The results are plotted in Figs. 4(d), (e), (f), together with those by the RTM method. Both lines agree fairly well. The depth of the dip is $2G_0$ in contrast to $1G_0$ for $N=6$, because we have two sets of coupled modes; $(1, -2)-(1, +3)-(2, -2)$ and $(1, +2)-(1, -3)-(2, +2)$. In the case of $N=7$, since no lower energy states satisfy Eq. (10), an energy gap does not appear.

In conclusion, we have calculated quantum conductance of the N -fold helical metallic nanowires by using the RTM method. We found that characteristic features appeared in the calculated conductance curves when the helical pitch L_H was in a certain range. By diagonalizing the model Hamiltonian, we showed that an energy gap appears due to a noncircular cross section of the wire when L_H is smaller than a critical pitch L_H^c . The condition for the appearance of the gap is $m - m' \equiv 0 \pmod{N}$, where m and m' are angular momentum quantum numbers. The gap shifts toward higher energies as the pitch L_H decreases, restoring the conductance of a cylinder in lower energies. Thus the anomalous conductance in these energies is observed only in a certain range of the pitch L_H ($\leq L_H^c$). In case of the gold nanowires of averaged radius $R=0.53$ nm, L_H^c was calculated to be 3.49 nm ($N=5$) or 11.33 nm ($N=6$). The geometry on which such anomalous conductance curves are expected may possibly be fabricated by the present nanometer technology. In the near future the modulation of the quantum conductance will be realized by controlling L_H , for example, by rotating the electrode, which may open the way to the quantum switch.

The authors would like to thank Y. Kondo, J. A. Torres, E. Tosatti, K. Terakura, T. Tonegawa, M. Kaburagi, and S. Hayashi for valuable discussions. This work was supported by New Energy and Industrial Technology Development Organization (NEDO).

¹Y. Kondo and K. Takayanagi, *Science* **289**, 606 (2000).

²O. Gülseren, F. Ercolessi, and E. Tosatti, *Phys. Rev. Lett.* **80**, 3775 (1998).

³E. Tosatti, S. Prestipino, S. Kostlmeier, A. Dal Corso, and F.D. Di Tolla, *Science* **291**, 288 (2001).

⁴R. Saito, M. Fujita, G. Dresselhaus, and M.S. Dresselhaus, *Phys. Rev. B* **46**, 1804 (1992).

⁵N. Hamada, S. Sawada, and A. Oshiyama, *Phys. Rev. Lett.* **68**, 1579 (1992).

⁶J.W.G. Wildoer, L.C. Venema, A.G. Rinzler, R.E. Smalley, and C. Dekker, *Nature (London)* **391**, 59 (1998).

⁷T.W. Odom, J. Huang, P. Kim, and C.M. Lieber, *Nature (London)* **391**, 62 (1998).

⁸J.A. Torres and J.J. Sáenz, *Phys. Rev. Lett.* **77**, 2245 (1996).

⁹J.M. van Ruitenbeek, M.H. Devoret, D. Esteve, and C. Urbina, *Phys. Rev. B* **56**, 12 566 (1997).

¹⁰E.N. Bogachek, A.G. Scherbakov, and U. Landman, *Phys. Rev. B* **56**, 1065 (1997).

¹¹F. Kassubek, C.A. Stafford, and H. Grabert, *Phys. Rev. B* **59**, 7560 (1999).

¹²Y.V. Sharvin, *Zh. Éksp. Teor. Fiz.* **48**, 984 (1965) [*Sov. Phys. JETP* **21**, 655 (1965)].

¹³K. Hirose and M. Tsukada, *Phys. Rev. B* **51**, 5278 (1995).

¹⁴M. Okamoto and K. Takayanagi, *Phys. Rev. B* **60**, 7808 (1999).

¹⁵E. Tekman and S. Ciraci, *Phys. Rev. B* **43**, 7145 (1991).